Distinct Metal−Thiolate Clusters in the N-Terminal Domain of Neuronal Growth Inhibitory Factor†

Peter Faller and Milan Vašák*

Biochemisches Institut der Universität Zürich, Winterthurerstrasse 190, CH-8057 Zürich, Switzerland

Received May 21, 1997; Revised Manuscript Received August 1, 1997⊗

ABSTRACT: Neuronal growth inhibitory factor (GIF), a brain-specific metallothionein-like protein (metallothionein-3), impairs the survival and neurite formation of cultured neurons. The metal distribution in isolated Cu_4,Zn_3−GIF is not known. In the present studies, the metal−thiolate clusters formed with monovalent and divalent metal ions in the N-terminal domain of human GIF [GIF(1−32)] were investigated. The cluster formation was followed by using electronic absorption, circular dichroism (CD), and magnetic circular dichroism (MCD), and in the case of Cu(I) complexes also by luminescence spectroscopy at 77 K. With Cu(I) ions, two well-defined clusters are formed involving the nine cysteine ligands of GIF-(1−32), i.e., Cu_4S_9- and Cu_6S_9-clusters. In contrast to the Cu_6S_9-cluster, the Cu_4S_9-cluster shows a remarkable stability to air oxidation. As similar properties and spectral features have also been observed with isolated Cu_{4-5},Zn_{2-3}−GIF, the presence of a Cu_4-cluster in this GIF form is suggested. The studies with Zn(II), Cd(II), and Co(II) ions indicated the presence of a Me_3S_9-cluster in GIF(1−32). However, spectral features of these metal derivatives substantially differ from those reported for the corresponding Me_3S_9-cluster in the β-domain of metallothioneins, suggesting structural differences. A large conformational flexibility of the Zn_3− and Cd_3−GIF(1−32) structures, characterized by short T_2 proton relaxations, precluded their investigation by NMR methods. The significance of Cu- and Zn-clusters for the structure of biologically active GIF(1−32) is discussed.

Alzheimer's disease (AD)[1] is characterized by progressive loss of neurons and the accumulation of senile plaques and neurofibrillary tangles in the brain (*1*). It has been found that a brain extract of AD victims shows enhanced neurotrophic activity promoting cortical neuron survival and dendrite outgrowth in the cell culture studies (*2, 3*). Further studies demonstrated that this enhanced neurotrophic activity is due to the down-regulation of a neuronal growth inhibitory factor (GIF). The characterization of GIF revealed a metalloprotein of 68 amino acids containing 4 copper and 3 zinc ions (*2*). The amino acid sequence of human GIF exhibits about 70% sequence identity with those of mammalian metallothioneins (MTs) including the preserved array of 20 cysteines. Similar amino acid sequences have been reported for GIF from rat, equine, and bovine brain (*4, 5*). When compared to MTs, the consensus GIF sequence shows two inserts: a Thr at position 4 and an acidic hexapeptide in the C-terminal region. An additional striking feature of the GIF sequence is the presence of two conserved proline residues comprised in the C(6)-P-C-P(9) motif. Molecular biological studies revealed that the GIF gene has a similar size, shares intron/exon boundaries, and is clustered on the same chromosome as MTs (MT-1, MT-2 isoforms). Based on these features, the GIF belongs to the superfamily of MTs and was classified as MT-3 (*5*).

Mammalian MTs are ubiquitous 61 amino acid proteins which bind d^{10} metal ions such as Zn(II), Cd(II), Cu(I), and Hg(II) in metal−thiolate clusters (*7*). The structure of MT with seven Zn(II) and/or Cd(II) ions has been solved in solution by NMR and in crystals by X-ray diffraction (*8*). Both the solution NMR structure and the X-ray structure reveal identical metal−thiolate cluster structures and a closely similar global polypeptide fold. In the MT structure, the N-terminal β-domain (amino acids 1−31) encompasses the $Me^{II}{}_3S_9$-cluster and the C-terminal α-domain the $Me^{II}{}_4S_{11}$-cluster. Despite high similarities between the primary structures of GIF and mammalian MTs, the biological properties of these proteins differ. MTs are predominantly expressed in parenchymatous tissues and are believed to play a role in the homeostasis of the essential trace metals (Zn, Cu), in the heavy-metal detoxification (Cd, Hg), and in the protection against oxidative stress (*9*). In contrast, GIF is expressed exclusively in the brain and exhibits its biological activity in this tissue. Furthermore, GIF mRNA levels were unaffected by the administration of heavy metals and other potent inducers of MT biosynthesis. Most importantly, in neuronal cell culture studies only GIF but not MTs exhibit a growth inhibitory activity (*2, 6*). This suggests that substantial differences between the structures of both proteins exist.

At present, the role of metal ions in GIF is not clear. In the original studies by Uchida et al. (1991) (*2*), human GIF isolated with four Cu and three Zn was identified as the biologically active form. Independent studies on bovine Cu_{4-5},Zn_{2-3}−GIF confirmed the presence of both metal ions, suggesting their functional importance. Moreover, it has been demonstrated that 4−5 copper and 2−3 zinc ions in

† This work was supported by Swiss National Science Foundation Grant 31-49460.96 and the EMDO Stiftung.

* To whom correspondence should be addressed at the Biochemisches Institut der Universität Zürich, Winterthurerstrasse 190, CH-8057 Zürich, Switzerland. Fax: (+41)-1-635 6831.

⊗ Abstract published in *Advance ACS Abstracts,* October 1, 1997.

[1] Abbreviations: AD, Alzheimer's disease; EXAFS, extended X-ray absorption fine structure; GIF, growth inhibitory factor; GIF(1−32), acetylated peptide from amino acids 1−32 of GIF; MT, metallothionein; CD, circular dichroism; MCD, magnetic circular dichroism; LMCT, ligand-to-metal charge-transfer; XAS, X-ray absorption spectroscopy.

S0006-2960(97)01199-9 CCC: $14.00

the bovine protein are organized in 2 independent metal−thiolate clusters with copper being present in a diamagnetic Cu(I) oxidation state (*10*). The biological activity of the recombinant human GIF forms has also been studied. Thus, a GIF form expressed in the zinc-containing *E. coli* culture exhibited a substantially lower biological activity (ca. 10%) compared to native Cu,Zn−GIF (*11)*. Independently, while the biological activity of the well-defined reconstituted Zn_7−GIF form was observed, the reconstituted GIF complexes containing Cu(I) or both Cu(I) and Zn(II) ions were found cytotoxic to neurons. In this case, recombinant human GIF was expressed in *E. coli* culture as the neurotoxic Cd-protein and subsequently reconstituted with the corresponding metal ions (*12*). Hence, it appears that all the reconstituted proteins were either toxic or, based on the studies by Tsuji et al. (1992) (*11),* less active.

Recent studies have shown that the N-terminal metal-containing peptide of GIF is sufficient for the growth inhibitory activity (*12*, *13*). The N-terminal part of GIF was identified to be responsible for the biological activity by two different approaches. First, native Cu,Zn−GIF was subjected to a limited digestion with proteases and the isolated 1−26-peptide, containing two Cu and one Zn, was found as active as native Cu,Zn−GIF. Moreover, it has been concluded that a correctly folded structure develops upon metal binding (*13*). Independently, the chemically synthesized N-terminal peptide of human GIF (amino acids 1−32), reconstituted with three Zn(II) ions, exhibited a similar level of biological activity when compared to that obtained with the reconstituted Zn_7−GIF form. By mutating the conserved C(6)-P-C-P(9) sequence to C-S-C-A or C-T-C-T, the biological activity of the zinc-containing peptide has been abolished. Based on this effect and the similar stoichiometry and reactivity of Zn_3−GIF(1−32) when compared to the β-domain of MT, it has been concluded that the observed loss of activity is due to local structural changes in the N-terminal domain and not due to unusal metal binding properties (*12*).

However, local changes in the surface topology of the Zn_3−GIF domain may not be the only cause for the loss of biological activity upon mutations. Alternatively, a change of the entire polypeptide fold of this domain brought about by the altered metal organization is evenly likely. The mutated sequence C-S-C-A occurs in a majority of mammalian MT sequences including those of rat, rabbit, and human. For these MTs, the three-dimensional structure has been determined and the identical cluster organization established (*8*). Hence, the mutation of the C-P-C-P sequence to C-S-C-A changes the GIF domain to that found in MTs which have been shown to be biologically inactive. In this context, the unusual properties of the MT structure should be briefly summarized. Thus, in contrast to a majority of apometalloproteins, in which the metal binding sites are preformed, the metal-free MT (apoMT) possesses a predominantly disordered structure. A well-defined, yet altered MT fold develops upon binding of monovalent or divalent metal ions to the apoprotein. This is exemplified by the existence of different metal−thiolate cluster structures with seven divalent metal ions [Zn(II), Cd(II)] compared to those with monovalent Cu(I) ions, where even two forms were found in nature, i.e., $Cu(I)_8$−MT and $Cu(I)_{12}$−MT (*14*, *15*). From this observation and other studies, it has been concluded that an interplay between both the chemistry of metal ions and the steric requirements of the polypeptide chain is responsible for the diversity of cluster structures in MT (*16*). Thus, a steric strain imposed by prolyl residues in the unique C-P-C-P sequence of GIF(1−32) together with other changes in the primary structure can lead to a different cluster organization and, hence, polypeptide fold of the GIF-(1−32) domain when compared to that in mammalian MTs.

For reasons stated above, it is not sufficient to determine just the stoichiometry of different metal ions bound when studying the relationship between the protein or peptide structure and biological activity. Clearly, knowledge of the cluster structure in the GIF(1−32) domain formed with divalent and monovalent metal ions as well as its natural metal occupation is essential for an understanding of the functional role of metal ions in this protein. In the present study, the biological active N-terminal part of human GIF (GIF 1−32) was chemically synthesized, and its complexes formed with both monovalent and divalent metal ions were examined. The metal complexes formed were characterized by using electronic absorption, circular dichroism (CD), magnetic circular dichroism (MCD), and luminescence spectroscopy. The results are compared with the corresponding spectroscopic data obtained on native Cu,Zn−GIF (*10*). Moreover, the first NMR characterization of the Zn-(II)- and Cd(II)-containing GIF(1−32) domain is presented.

MATERIALS AND METHODS

Preparation of N-Terminal Peptide (GIF 1−32) and Its Metal Derivatives. (A) Peptide Synthesis and Purification. The N-terminal half of human GIF (residues 1−32, N-terminal acetylated) was synthesized by standard Fmoc chemistry on an ABI 433 A peptide synthesizer. The synthesized peptide possesses the following amino acid sequence: Ac-M-D-P-E-T-C-P-C-P-S-G-G-S-C-T-C-A-D-S-C-K-C-E-G-C-K-C-T-S-C-K-K. A 0.1 mmol peptide synthesis was carried out using cleavage conditions recommended by the manufacturer. The GIF(1−32) peptide was purified by desalting over a gel filtration column (G-10, 10 mM HCl) followed by two successive C_{18} reverse-phase HPLC steps on a semipreparative column (Brownlee Aquapore ODS 300, 0.4 × 22 cm) (*12*). Electrospray mass spectrometry (Sciex API III$^+$) of the purified GIF(1−32) yielded a mass of 3305.2 Da, which agreed well with the calculated mass of 3305.8 Da.

(B) Metal Derivatives of GIF(1−32). All solutions used in the preparation of the Co(II)− or Zn(II)−, Cd(II)−, and Cu(I)−GIF(1−32) derivatives were rendered oxygen-free by degassing on a vacuum line using freeze−pump−thaw cycling, and all manipulations were carried out in an argon- or nitrogen-purged glovebox. In the titration of the peptide with the metal ions, each titration step represented an independently prepared sample. Prior to mixing of the peptide with the required metal ions, the metal concentration of the freshly prepared stock solution was determined by atomic absorption spectroscopy (IL Video 12) and that of the peptide via sulfhydryl concentration (nine Cys per peptide). In the latter case, the sulfhydryl reaction with 2,2′-dithiopyridine in 0.2 M sodium acetate (pH 4) was followed spectroscopically and the concentration determined using ϵ_{343} = 7600 M^{-1} cm^{-1} (*17*). Following the spectroscopic measurements, the metal to GIF(1−32) ratios were checked again using a small aliquot of the sample. The individual metal derivatives of GIF(1−32) were prepared as follows.

The Cd(II)− and Zn(II)−GIF(1−32) forms were generated by the addition of desired equivalents of $Me^{II}Cl_2$ solution to GIF(1−32) in 10 mM HCl followed by pH adjustment to 7.0 with 0.5 M Tris base (Trizma from Sigma). Co_3−GIF-(1−32) was obtained by mixing 3 equiv of $CoCl_2$ with GIF-(1−32) in 0.1 M HCl. The solution mixture was then adjusted to pH 8.3 with 1 M Tris base. The Cu(I)−GIF-(1−32) complexes were prepared by offering known equivalents of Cu(I) ions, as the stable $[Cu^I(CH_4CN)_4]ClO_4$ complex (*18*) in 5 mM HCl/20% acetonitrile, with stirring to the apopeptide in 10 mM HCl/5% acetonitrile. Subsequently, the pH was raised to 7.4 with 0.5 M Tris base. Since only the metal concentration but not the peptide concentration could be determined upon Cu(I) binding to the peptide [Cu-(I) cannot be easily released from the peptide], each titration step has been performed at least in duplicate. Similar experiments in the absence of protein established that no absorption of the Cu(I)−acetonitrile complex is observed in the spectral region studied. The absence of any Cu(II) in the freshly prepared Cu(I) stock solution (ca. 20 mM) was confirmed by EPR measurement. The EPR spectrum was recorded with a Varian E6 spectrometer at 90 K using gaseous nitrogen and a variable-temperature controller (Varian).

Spectroscopic Measurements. Absorption spectra were recorded on a Cary 3 spectrometer. CD and MCD measurements were made using a Jasco (Model J-715) spectropolarimeter equipped with a 1.5 T electromagnet for room temperature MCD measurements. The CD spectra are expressed as molar ellipticity, θ, in units of deg $dmol^{-1}$ cm^{-1} and the MCD spectra as, θ_M in units of deg $dmol^{-1}$ cm^{-1} T^{-1}. Luminescence spectra at 77 K and decay data were obtained using a SPEX fluorolog spectrofluorometer fitted with the 1934C phosphorimeter accessory using a 45° detection geometry. The samples were placed into 2 mm i.d. quartz tubes and immersed in a cylindrical quartz Dewar vessel filled with liquid nitrogen. Luminescence spectra were recorded at 77 K on the microcrystalline frozen samples using a 50 ms delay and a 0.3 ms acquisition window. The excitation wavelength was 300 nm. ^1H NMR spectra were recorded on Bruker AMX-600 and/or AMX-300 spectrometers. All NMR samples (1 mM) contained 10% ^2H_2O to provide the field-frequency lock and were measured in 5 mm NMR tubes.

RESULTS AND DISCUSSION

Both native Cu,Zn−GIF and the reconstituted Zn_7−GIF were found biologically active. However, no comparative biological studies on well-defined metal derivatives are currently available. To aid our further studies on GIF, we examined the cluster structures formed with the GIF(1−32) peptide when monovalent or divalent metal ions were offered.

Cu(I)−GIF-Containing Forms

Absorption Spectra of Cu_4− and Cu_6−GIF(1−32) Forms. At present, no three-dimensional structure of Cu(I)−thiolate clusters in proteins exists. However, using various spectroscopic techniques such as electronic absorption, CD, MCD, luminescence, XAS, and EXAFS, structural features of Cu-(I)−thiolate clusters in a number of proteins, e.g., transcription factors, ACE, MTs, and related proteins, have been obtained (*19, 20, 21, 22, 23*). The former four techniques were also used in the present studies.

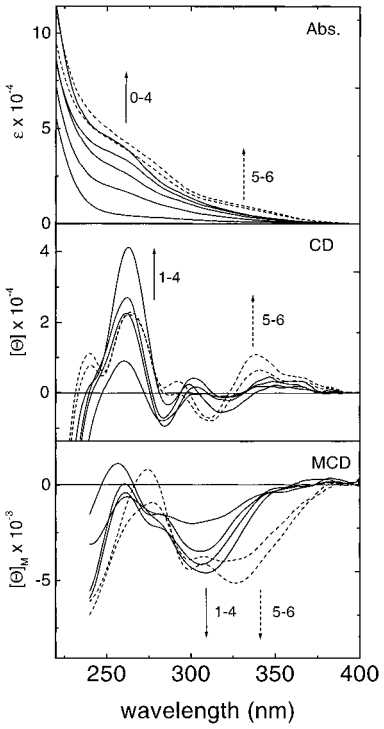

FIGURE 1: Electronic absorption (Abs.), circular dichroism (CD), and magnetic circular dichroism (MCD) spectra of the GIF(1−32) domain recorded as a function of increasing mole equivalents of Cu(I) at pH 7.4. Arrows indicate increasing Cu(I) equivalents present in the individual samples (solid line): 0, 1.4, 2.1, 2.9, 3.9; (dashed line) 5.3, 6.4. For details regarding the sample preparations and the determination of the GIF(1−32) to metal ratios, see Materials and Methods.

In order to examine the binding capacity of GIF(1−32) with Cu(I) ions, the complexes formed with differing mole equivalents of copper were spectroscopically characterized. The absorption spectra of Cu(I)−GIF(1−32) are characterized by the appearance of metal-dependent features starting at about 380 nm and extending into the far-UV. The broad absorption envelope shows a prominent shoulder around 262 nm and a weak shoulder at about 295 nm (Figure 1). The intensity of the 262 nm shoulder increases more or less linearly with increasing Cu(I) equivalents up to around 4 Cu(I) equiv. Further incremental addition of 2 Cu(I) equiv led mainly to a marked red shift of the spectral envelope characterized by two well-resolved shoulders at 280 and 340 nm. Above this titration point, no dramatic changes of the spectral profile occurred. The spectral changes are consistent with the formation of two Cu(I) complexes, i.e., Cu_4− and Cu_6−GIF(1−32). This is better documented in the corresponding CD and MCD spectra where well-resolved bands are present (Figure 1). The shape of the CD spectra is essentially unchanged up to about 4 Cu(I) equiv and is characterized by positive and negative extrema at (+)262 nm, (−)290 nm, (+)310 nm, (−)325 nm, and (+)350 nm. On going from 4 to 6 equiv of Cu(I), major changes in the position and the sign of the original extrema occurred, i.e., (+)262 nm, (+)292 nm, (−)313 nm, and (+)335. Similar spectral behavior was also observed in the parallel MCD studies (Figure 1). No changes were discerned in the shape up to 4 Cu(I) equiv with extrema at (+)256 nm and (−)307 nm and a shoulder at (−)280 nm. With 6 Cu(I) equiv, these features underwent a red shift to (+)273 nm and (−)328 nm and a shoulder to (−)296 nm. Thus, all spectroscopic

results clearly indicate the generation of the Cu_4− and Cu_6−GIF(1−32) forms. Moreover, since the spectral features were essentially unchanged up to 4 Cu(I) equiv, it is concluded that the Cu_4−GIF(1−32) complex is formed in a cooperative fashion.

Further structural information about the Cu(I)−GIF(1−32) complexes formed relies on the knowledge of the spectral origin of the absorption, CD, and MCD spectra of Cu(I)−thiolate complexes. Such a detailed analysis exists for mammalian Cu(I)−MT (*23*). Thus, while the bands in the high-energy region (below 280 nm) originate predominantly from CysS−Cu(I) LMCT transitions, the features in the low-energy region with very weak molar absorptivities, but rather strong CD and MCD bands, originate from formally spin-forbidden 3d → 4s metal cluster-centered transitions brought about by Cu(I)−Cu(I) interactions in polynuclear Cu(I) complexes. Therefore, the presence of similar low-energy features in the Cu_4− and Cu_6−GIF(1−32) complexes indicates the existence of Cu(I) polyhedra (*23* and references therein). Since the high-energy region originates from LMCT transitions, the intensity of the 262 nm shoulder should reflect the number of thiolate ligands involved in metal binding. Using the molar absorptivity of ca. 5500 M^{-1} cm^{-1} per cysteine thiolate at 262 nm (*23*), the number of cysteine ligands in the Cu_4−GIF(1−32) cluster can be estimated. The magnitude of the 262 nm feature ($\epsilon_{262} \approx$ 43 000 M^{-1} cm^{-1}) suggests the involvement of about 8−9 thiolates and hence the existence of a $Cu_4(CysS)_{8-9}$ cluster. This indicates that in the Cu_4-cluster all nine cysteines of the GIF(1−32) peptide take part in the Cu(I) coordination. Supporting evidence for the lack of free thiolate groups in this species is provided by the absence of a modification reaction with 2,2′-dithiopyridine (see above). Consequently, an additional binding of the 2 Cu(I) equiv giving rise to a new $Cu_6(CysS)_9$ cluster must be accompanied by a substantial structural rearrangement of the original $Cu_4(CysS)_9$ cluster. This is illustrated by dramatic changes of the cluster centered transitions (above 280 nm) in both CD and MCD spectara (Figure 1). In addition, in the C-T region the corresponding spectral features of Cu_6−GIF(1−32) are markedly red shifted, suggesting that the nature of the thiolate ligands differs. By analogy with previous studies on MTs (*26, 27*), we attribute this spectral behavior to a Cu(I) coordination by predominantly bridging thiolates, due to their relatively lager polarization when compared with that of terminal thiolates. The red shift is also responsible for an apparent small intensity increase of the absorption envelope at 262 nm. At this point, it should be noted that such dramatic spectral changes are absent in MT on going from the Cu_4-cluster to the Cu_6-cluster since the number of thiolate ligands involved in Cu(I) coordination increases. The participation of all 20 cysteines of MT in metal binding occurs with 12 Cu(I) ions giving rise to 2 Cu_6-clusters, i.e., Cu_6S_9 and Cu_6S_{11}. Note that the formation of the Cu_6S_9-cluster in the β-domain of MT has also been shown (*20, 21*). However, the formation of 2 Cu_4-clusters in this protein with 8 Cu(I) requires only 12−14 cysteine ligands; i.e., 2 Cu_4S_{6-7} clusters are generated (*23*). Thus, the formation of the Cu_4S_9-cluster in GIF(1−32) is unique to this protein (see below.).

Luminescence Spectra of *Cu_4− and Cu_6−GIF(1−32) Forms.* The widely differing low-temperature (77 K) spectra of Cu_6− and Cu_4−thiolate clusters have been used to differentiate between the formation of these cluster forms in Cu(I)−MT. Thus, while the former cluster exhibited only a single emissive band at 600 nm, in the case of the Cu_4-cluster two emissive bands at 610 and 420 nm have been found (*23*). These emissions arise from two distinct triplet excited state manifolds which are mixed LMCT/d-s transitions in origin (*23, 24*). The 420 nm emissive band of the Cu_4-cluster has been attributed to a cluster centered in origin, being delocalized over the metal core. The 600 nm emissive band is predominantly composed of ligand p orbitals. Both the lifetimes of the emission bands at 600 and 420 nm of ca. 130 and 50 ms, respectively, together with a large Stoke's shift are consistent with their originating from triplet excited states (*23*).

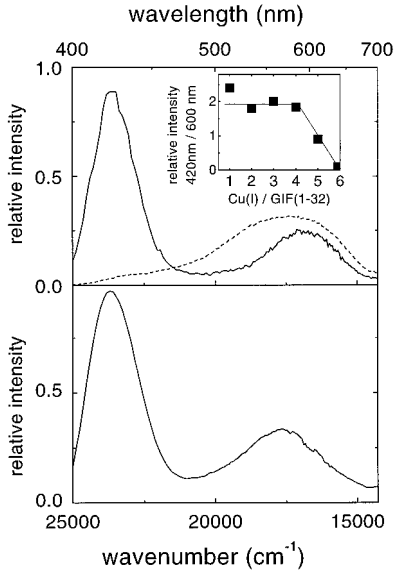

FIGURE 2: (Top) Phosphorescence spectra of Cu_4−GIF(1−32) (solid line) and Cu_6−GIF(1−32) (dashed line) at 77 K. The inset panel illustrates the effect of the Cu(I):apo−GIF(1−32) ratio on the relative emission intensity ratio 420/600 nm. (Bottom) For comparison, the phosphorescence emission spectrum of native Cu_{4-5},$Zn_{2-2.5}$−GIF at 77 K is presented (*10*). Excitation wavelength at 300 nm. For details, see text.

The 77 K emission spectra of the Cu_4− and Cu_6−GIF-(1−32) complexes are illustrated in Figure 2 (top). Both spectra show a broad emission band around 590 nm, but only in the case of the Cu_4 complex was a second emission band at 420 nm discerned. The high- as well as the low-energy emission decayed in all Cu(I) titration steps according to a single exponential function with lifetimes (τ) of ca. 30 and 120 ms, respectively. The similar lifetimes of these bands throughout the titration allow a comparison of their intensity. Both the spectral profile and the intensity ratio of 420 and 590 nm bands were unchanged with up to 4 Cu(I) equiv added to the peptide. Further Cu(I) addition gradually diminished the high-energy band, being absent with 6 Cu(I) equiv (Figure 2, inset). These results are in full agreement with the above conclusion of two Cu(I)−thiolate cluster forms with the Cu_4-cluster being formed cooperatively. It should be noted that using room temperature luminescence, which has been applied to establish the binding capacity of GIF(1−32) with the Cu(I) ions, only the formation of the Cu_6-cluster has been observed (*12*).

Comparison of the Cu_4−GIF(1−32) Cluster with Native Cu,Zn−GIF. For native Cu_{4-5}, Zn_{2-3}−GIF, it has been suggested that the four Cu(I) and three Zn(II) ions are

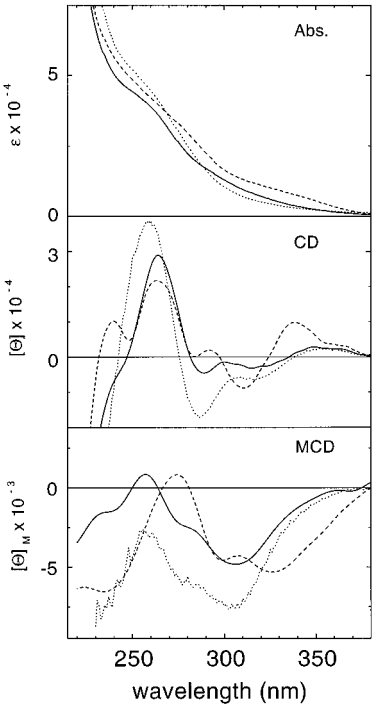

FIGURE 3: Comparison of the electronic absorption (Abs.), circular dichroism (CD), and magnetic circular dichroism (MCD) spectra of Cu_4−GIF(1−32) (solid line) and Cu_6−GIF(1−32) (dashed line) with those reported for native $Cu_{4-5}Zn_{2-2.5}$−GIF (dotted line) (*10*).

organized in two independent metal−thiolate clusters. In this protein, the spectral contribution of the zinc−thiolate cluster occurs below 250 nm and that of the copper−thiolate cluster mainly above 250 nm (*10*). Hence, the spectral features of the copper−thiolate cluster in native Cu,Zn−GIF can be compared with those of the Cu_4−GIF(1−32) cluster. Note that the spectral features of the Cu_6−GIF(1−32) cluster widely differ (see Figures 1 and 3). As illustrated in Figures 2 and 3, there is a close correspondence between the absorption, CD, MCD, and luminescence spectra of the Cu_4−GIF(1−32) cluster and that present in native Cu_{4-5},Zn_{2-3}−GIF. It may be noted that similar lifetimes for both emission bands of Cu,Zn−GIF were obtained, *ca.* 40 and 150 ms for the high- and the low-energy band, respectively, when compared with those of the Cu_4−GIF(1−32) cluster (see above). Thus, the similarity between the spectral features of the Cu_4−GIF(1−32) cluster and native Cu,Zn−GIF strongly suggests the presence of the Cu_4S_9 cluster in this protein. This conclusion is supported by the fact that the four Cu(I) ions in native Cu,Zn−GIF are also coordinated by approximately nine cysteines (*10*).

The striking feature of native Cu,Zn−GIF is its stability against air oxidation (*10*). This behavior is quite unusual for Cu(I)−thiolate clusters. The instability of mammalian Cu(I)−MTs in air is well documented (*20*). An increased stability has so far been reported only for Cu(I)−MT from yeast (*25*). Therefore, the stability in air of both Cu(I)-clusters formed with GIF(1−32) was examined. Upon exposure of nitrogen-saturated Cu_4−GIF(1−32) solution to air, the electronic absorption spectrum did not show any changes in shape or intensity over a time period of 12 h. In contrast, with the $Cu(I)_6$−GIF(1−32) form, gradual spectral changes occurred with time in both shape and intensity. Already after 30 min exposure to air a marked intensity decrease of the absorption bands at 245 and 320 nm has been seen (data not shown). Thus, the unusual stability of Cu,-Zn−GIF in air is preserved in the Cu_4−GIF(1−32) form.

Zn(II)−, Cd(II)−, and Co(II)−GIF(1−32) Derivatives

As mentioned above, both zinc-reconstituted GIF forms, i.e., Zn_3−GIF(1−32) and the recombinant Zn_7−GIF(1−32), have shown a similar biological activity. To learn more about the cluster structure in GIF(1−32) with divalent metal ions, besides the Zn_3−GIF(1−32) form also the Cd_3−GIF-(1−32) form was studied. The spectroscopic characterization of the Cd−GIF(1−32) form should provide the basis for structural investigations by NMR. The use of ^{113}Cd NMR proved to be indispensable in the solution structure determination of MTs (*8*).

Zn(II)−GIF(1−32) Derivatives. GIF(1−32) binds up to three Zn(II) ions as determined by offering an excess of Zn(II) ions (4-fold) to the peptide followed by gel filtration chromatography. The same stoichiometry for this form has also been found by Sewell et al. (*12*). Apo−GIF(1−32) shows an unresolved tailing in the electronic absorption starting at 240 nm and extending into the far-UV region. The Zn_3−GIF(1−32) form showed a similar unresolved absorption profile between 210 and 240 nm but with a gradually increasing intensity into the high-energy region. In the corresponding CD spectrum, the Zn_3−GIF(1−32) form is dominated by a broad positive CD band centered at about 223 nm with tailing to 250 nm (data not shown). By analogy with similar spectral features reported for Zn_7-MT (*26*), both the absorption and CD spectra of Zn_3−GIF(1−32) are dominated by CysS−Zn(II) LMCT transitions consistent with the Zn(II)−thiolate ligations. However, in Zn_7−MT, the maximum of a broad positive CD band occurred at about 242 nm (*26*).

Cd(II)−GIF(1−32) Derivative. Similarly to the zinc form, the addition of an excess of Cd to GIF(1−32) (4-fold) followed by gel filtration resulted in Cd_3−GIF(1−32). Due to the increased covalence of the Cd−S bonds, the LMCT bands of Cd(II)−thiolate complexes are red shifted compared to those of Zn−S complexes and are, therefore, better accessible to spectroscopic studies. Figure 4 shows the changes in electronic absorption, CD, and MCD spectra brought about by the incremental addition of Cd(II) to apo-GIF(1−32). In the absorption spectra, a shoulder at about 250 nm increases almost linearly with the first 2 Cd(II) equiv. Upon the addition of the last Cd(II) equiv, a substantially smaller increase in intensity was observed. Examination of the low-energy tailing of these absorption bands reveals that the gradual red shift of this feature as a function of Cd(II) addition is due to an increasing absorption in this spectral region. As has been demonstrated in the case of Cd−MTs, similar Cd-induced spectral features above 220 nm originate from the CysS−Cd LMCT transitions of the Cd−thiolate clusters, with transitions from bridging thiolate ligands being red shifted when compared to those from terminal thiolates (*27*). Thus, the increase of the low-energy absorption during the Cd titration of GIF(1−32) suggests that an increasing number of bridging thiolates are involved. This is supported by the corresponding MCD spectra where a gradual red shift of both MCD bands with increasing Cd increments is seen (Figure 4); the well-resolved negative MCD extremum shifts from 253 to 260 nm. In the

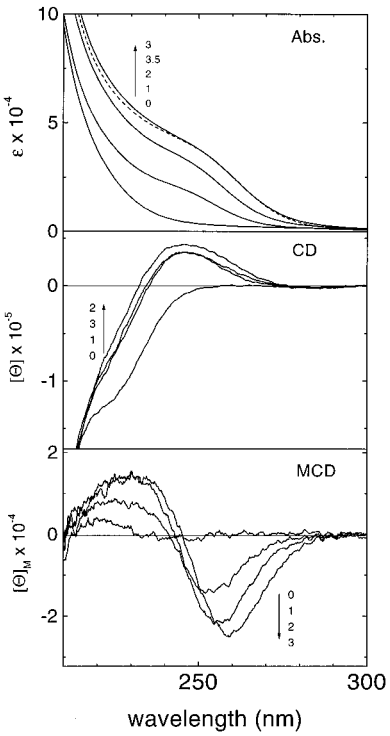

FIGURE 4: Electronic absorption (Abs.), circular dichroism (CD), and magnetic circular dichroism (MCD) spectra of the GIF(1−32) domain recorded as a function of increasing mole equivalents of Cd(II) at pH 7.0. Arrows indicate increasing Cd(II) equivalents present in the individually prepared samples (solid line): 0, 1, 2, 3; (dashed line) 3.5. For details regarding the sample preparations and the determination of the GIF(1−32) to metal ratios, see Materials and Methods.

corresponding CD spectra of Cd−GIF(1−32), characterized by a CD band at (+)246 nm with a tailing to about 270 nm, the positive CD band reaches the maximum intensity with approximately 2 Cd(II) equiv and decreases upon binding of the third Cd(II) equiv. This behavior indicates that substantial structural changes occur during the formation of the Cd_3-cluster. Thus, in contrast to the cooperative formation of the Cu_4-cluster, the Cd_3-cluster is formed in a noncooperative fashion.

Comparison between the Cd_3−GIF(1−32) Cluster and the Cd_3-Cluster in the β-Domain of Mammalian MTs. In all structurally characterized mammalian Cd_7−MTs, the three Cd(II) ions in the β-domain (residues 1−31) are organized in a cyclohexane-like Cd_3S_9-cluster. Cd binding to the individual β-domain of human and calf MTs has also been studied by CD spectroscopy, with CD features of the Cd_3-containing β-domains being qualitatively closely similar in shape and intensity (*28*, *29*). The Cd_3-cluster in the human β-domain shows a broad positive CD envelope between 300 and 230 nm characterized by two partially resolved CD bands at 250 and 275 nm of comparable intensity (*28*). Note that mammalian Cd_7−MTs are characterized by a biphasic CD profile with CD extrema at about (+)260 and (−)239 nm originating from an excitonic coupling between transition dipole moments of bridging thiolate ligands (*27*) within the Cd_4−thiolate cluster (*29*). Thus, in contrast to the CD spectrum of the Cd_3-containing β-domain, the Cd_3−GIF(1−32) cluster displays only a single positive CD band at 246 nm (Figure 4). In addition, the intensity of the CD band at (+)246 nm is about twice as high compared with that reported for the CD features of the Cd_3-containing β-domain (*28*, *29*). Overall, the marked CD dissimilarities between the Cd_3−GIF(1−32) and the Cd_3-containing β-domain of MTs suggest that substantial differences between these structures exist.

NMR Studies of Zn_3− and Cd_3−GIF(1−32). The three-dimensional structure of the biologically active GIF(1−32) domain by NMR methods should provide a better understanding of the structure−function correlation of GIF. With this aim, we have initiated ^{1}H NMR studies of apo−GIF(1−32) and Zn_3− and Cd_3−GIF(1−32). The one-dimensional ^{1}H NMR spectrum of apo−GIF(1−32) in H_2O (20 mM phosphate buffer, 100 mM NaCl, pH 5.5) revealed sharp proton resonances in both the high- and low-field regions. In the low-field region, all the amide proton resonances occurred at about 8.2 ppm, suggesting that the metal-free peptide possesses predominantly a disordered structure (not shown). Note that aromatic amino acids and histidine are absent in GIF. In both Zn_3− and Cd_3−GIF(1−32), the increased chemical shift dispersion of the amide resonances between 7 and 9.2 ppm indicated the presence of a structure developing upon metal binding (20 mM Tris-HCl-d_{11}, 100 mM NaCl). However, these NMR features appeared in both metalloderivatives as a broad, poorly resolved envelope with only a few more resolved NMR peaks. Similar broad features occurred also in the high-field region of the corresponding ^{1}H NMR spectra (not shown). Such a line broadening of all resonances would be anticipated with a protein of molecular mass of *ca.* 20 kDa and not with the *ca.* 4 kDa peptide complex. Consequently, this NMR feature is consistent with a short T_2 relaxation of the proton resonances in metal-containing GIF. In this case, the short T_2 relaxation may originate either from the high molecular weight (slow tumbling), from paramagnetic impurities, or from chemical exchange processes associated with a conformational flexibility of the structure. Aggregation as the reason for short T_2 proton relaxations could be excluded based on gel chromatography as both the NMR sample (ca. 1 mM) and the 10 times diluted sample showed a similar apparent molecular mass of about 6−7 kDa. Furthermore, based on the sharpness of the ^{1}H resonances originating from Tris buffer in the samples of Zn_3− and Cd_3−GIF(1−32), the effect of paramagnetic impurities as the cause for short T_2 relaxation could also be ruled out. Therefore, it appears that conformational flexibility of the structure is responsible for the signal broadening. With the aim to change the unfavorable time scale of this process, the ^{1}H NMR spectra of Cd_3−GIF(1−32) were recorded under different experimental conditions. However, the changes of temperature from 30 to 4 °C, salt concentrations between 20 and 200 mM (KCl or $MgSO_4$), pH values between 5.5 and 6.6 (phosphate buffers), and the presence of 50% methanol in the sample were without a substantial effect on the signal line widths. The reason for conformational flexibility of the structure is currently unknown. At present, we favor metal exchange processes in Zn_3− and Cd_3−GIF(1−32) as the cause for the structure fluxionality.

$Co(II)_3$−GIF(1−32) Derivative. Since no structural information about Cd_3−GIF(1−32) could be obtained from NMR, we have examined the corresponding Co(II) metal derivative. Owing to the d−d transitions, Co(II) is a sensitive probe regarding the coordination geometry of the Zn sites in proteins. Co_3−GIF(1−32) shows absorption bands in the d−d region between 450 and 800 nm. These bands originate

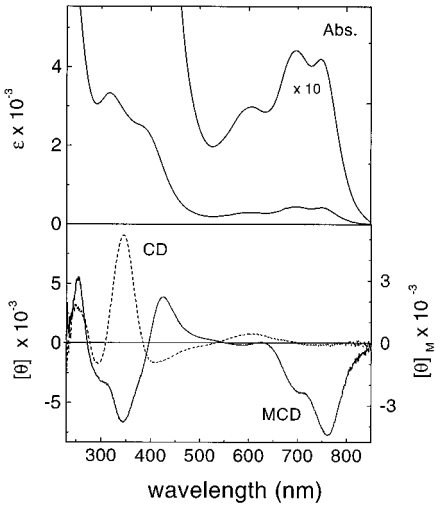

FIGURE 5: Absorption (Abs), circular dichroism (CD), and magnetic circular dichroism (MCD) spectra of Co^{II}_3−GIF(1−32) at pH 8.3. For details, see Materials and Methods.

from the spin-allowed υ_3 [$^4A_2 \rightarrow {}^4T_1(P)$] transition and are indicative of a tetrahedral tetrathiolate coordination (Figure 5) (*30, 31*). This conclusion is substantiated by the corresponding MCD spectrum (Figure 5) revealing a strong MCD band at (−)762 nm with a shoulder at 700 nm and weak bands at (−)620 and (+)580 nm. This MCD pattern is diagnostic of a T_d type of symmetry for the Co(II) sites (*32*). The CD spectrum is less informative. Evidence for the distortion from a T_d symmetry comes from the energy separation and the molar absorptivity of the spin−orbit coupling components of the υ_3 transition at 608, 697, and 752 nm of 330, 480, and 460 M^{-1} cm^{-1} per Co(II), respectively ($\epsilon > 250$ M^{-1} cm^{-1}) (*32*). In the high-energy region (below 450 nm), the band at 318 nm with a shoulder at 390 nm originates from CysS−Co(II) charge-transfer transitions. Similar bands have also been seen in a number of Co(II)−MT derivatives (*31*). The band at 318 nm shows a molar absorptivity of 3360 M^{-1} cm^{-1} per Co(II). The molar absorptivity of about 1100 M^{-1} cm^{-1} per Co(II)−thiolate bond is well established (*33*). Using this value, three cysteine ligands participate in Co(II) binding. However, to account for the tetrathiolate coordination and a total of nine cysteines, a Co(II)−thiolate cluster structure must be present in Co_3−GIF(1−32). Thus, similarly to Co_7−MT (*31, 34*), a Co_3S_9-cluster exists in GIF(1−32). However, the exact nature of this cluster structure remains undetermined. As no studies of the Co(II)-containing β-domain exist, the spectral features of Co_3−GIF(1−32) can be compared with those reported for Co_3,$^{113}Cd_4$−MT. In this case, the Co(II) ions are bound exclusively to the three-metal cluster of the N-terminal domain (amino acids 1−31) (*35*). The d−d profile of this cluster revealed absorption bands at 750, 686, and 586 nm with molar absorptivities per Co(II) being approximately 10% higher and blue shifted compared with those of Co_3−GIF(1−32) (see above). Based on the lower absorptivity and smaller energy separation of the spin−orbit coupling components, the Co_3S_9-cluster in GIF-(1−32) is substantially less distorted. However, it should be noted that although the metal binding domains in mammalian MTs are well separated, an effect of the C-terminal domain on the N-terminal Co_3S_9-cluster structure cannot be entirely ruled out.

CONCLUSIONS

The detailed spectroscopic studies of GIF(1−32) complexes formed with the divalent and monovalent metal ions suggest the presence of marked structural differences between these complexes and those reported for the β-domain of mammalian MTs. For the Zn_3−GIF(1−32) form, this conclusion is supported by our recent EXAFS studies on Zn_3−GIF(1−32) and the reconstituted Zn_7−GIF form in which an outer shell backscattering at *ca.* 3.28 Å, absent in Zn_7−MT, was found (unpublished data). Moreover, from the studies of Zn_3−GIF(1−32) and of the forms containing divalent metal ions commonly used to probe for these sites in proteins, i.e., Cd(II) and Co(II), it can be concluded that a Me_3S_9-cluster is formed with each metal ion being tetrahedrally coordinated by bridging and terminal thiolates. The participation of all cysteines of GIF(1−32) in metal binding suggests that a two-domain structure similar to that found in MTs also exists in this protein. A two-domain structure of GIF has also been inferred from the binding stoichiometries of 3 and 4 obtained with divalent metal ions for the isolated peptides GIF(1−32) and GIF(32−68), respectively (*12*). In the titration of GIF(1−32) with Cu(I), two well-defined complexes were formed, i.e., Cu_4S_9- and Cu_6S_9-clusters. The Cu_4S_9-cluster has not been formed in the β-domain of MT. The results suggest that a similar Cu_4S_9-cluster is also present in native Cu,Zn−GIF. Furthermore, based on the similar spectral characteristics of the Cu_4-cluster in GIF(1−32) and native Cu,Zn−GIF, it is reasonable to assume that the Cu(I) ions in native GIF are localized in the N-terminal metal binding domain. The stability of the Cu_4−GIF(1−32) and native Cu,Zn−GIF forms in air is highly unusual. In air-sensitive Cu(I)−MTs, the Cu(I) ions are digonally and trigonally coordinated (*20*). Similarly to the Cu_6S_9-cluster in the β-domain of MTs, the Cu_6S_9-cluster in GIF(1−32) is also air sensitive. Therefore, the formation of a stable Cu_4S_9-cluster in GIF(1−32) with an increased cysteine:metal ratio must give rise to a widely different Cu(I)−thiolate cluster structure. The simplest crystallographically defined inorganic model possessing a polynuclear Cu_4S_9-core is that of the Cu(I)−thiourea complex, i.e., $Cu_4[SC(NH_2)_2]_9^{4+}$. This structure is adamantane-like with one trigonal planar copper and three very distorted tetrahedral copper species (*36*). At present, we ascribe the air stability of the Cu(I)−GIF complex to geometrical constrains of the Cu_4−GIF(1−32) structure, which stabilize the Cu(I) oxidation state. In light of our findings, the reported toxicity of the reconstituted Cu,Zn−GIF form in neuronal cell culture studies by Sewell et al. (1995) (*12*) should also be discussed. The reconstituted Cu,Zn−GIF was generated by adding of 6 Cu(I) equiv to Zn_7−GIF. By analogy with MTs, one would expect that an air-sensitive $Cu(I)_6$-cluster is formed (*37*). The oxidation of Cu(I)−thiolate complexes occurs through a redox cycling. The released Cu(II) ions can then undergo various radical reactions like DNA cleavage (*38*). This could explain the observed toxicity of the reconstituted Cu,Zn−GIF form in cell culture and the absence of such a toxic effect in the case of native Cu,Zn−GIF containing the Cu_4−thiolate cluster. Thus, although in this study just the structural features of the metallic core of GIF(1−32) were examined, the results clearly demonstrate that the geometrical constraints imposed by the primary structure of GIF substantially

differ from those of mammalian MTs. In the MT structure, the interaction between both the metal ions and the polypeptide chain determines the final three-dimensional structure. Therefore, it is anticipated that the structural changes between the GIF and MT domains will be much more profound and not restricted to the postulated local structural change introduced by the C-P-C-P sequence of GIF(1−32). In addition, as copper in Cu_4−GIF(1−32) cannot isostructurally replace zinc in Zn_3−GIF(1−32), a total fold of this domain with both metal ions must also differ. Hence, further structural and biological studies of GIF are necessary to establish the role of metal ions in this protein.

ACKNOWLEDGMENT

We thank Dr. R. Bogumil for helpful discussion. The expert assistance of Dr. S. Klauser with the synthesis of the peptide and Dr. O. Zerbe in obtaining the NMR spectra is gratefully acknowledged.

REFERENCES

1. Selkoe, D. J. (1991) *Neuron 6*, 487−498.
2. Uchida, Y., Takio, K., Titani, K., Ichada, Y., and Tomonaga, M. (1991) *Neuron 7*, 337−347.
3. Erickson, J. C., Sewell, A. K., Jensen, L. T., Winge, D. R., and Palmiter, R. D. (1994) *Brain Res. 649*, 297−304.
4. Pountney, D. L., Fundel, S. M., Faller, P., Birchler, N. E., Hunziker, P., and Vašák, M.(1994) *FEBS Lett. 345*, 193−197.
5. Palmiter, R. D., Findley, S. D., Whitmore, T. E., and Durnam, D. M. (1992) *Proc. Natl. Acad. Sci. U.S.A. 89*, 6333−6337.
6. Erickson, J. C., Sewell, A. K., Jensen, L. T., Winge, D. R., and Palmiter, R. D. (1994) *Brain Res. 649*, 297−304.
7. Vašák, M., and Kägi, J. H. R. (1994) in *Encyclopedia of inorganic chemistry*. (King, R. B., Ed.) Vol. 4, pp 2229−2241, John Wiley & Sons Ltd., New York.
8. Braun, W., Vašák, M., Robbins, A. H., Stout, C. D., Wagner, G., Kägi, J. H. R., and Wüthrich, K. (1992) *Proc. Natl. Acad. Sci. U.S.A. 89*, 10124−10128.
9. Kägi, J. H. R. (1993) in *Metallothionein III* (Susuki, K. T., Kimura, M., and Imura, N., Eds.) pp 29−56, Birkhäuser, Basel.
10. Bogumil, R., Faller, P., Pountney, D. L., and Vašák, M. (1996) *Eur. J. Biochem. 238*, 698−705.
11. Tsuji, S., Koboyashi, H., Uchida, Y., Ihara, Y., and Miyatake, T. (1992) *EMBO J. 11*, 4843−4850.
12. Sewell, A. K., Jensen, L. T., Erikson, J. C., Palmiter, R. D., and Winge, D. R. (1995) *Biochemistry 34*, 4740−4747.
13. Uchida, Y., and Ihara, Y. (1995) *J. Biol. Chem. 270*, 3365−3369.
14. Hunziker, P. E., and Sternlieb, I. (1991) *Eur. J. Clin. Invest. 21*, 466−471.
15. Johnson, G. F., Morrell, A. G., Stockert, R. J., and Sternlieb, I. (1981) *Hepatology 1*, 243−248.
16. Vašák, M., and Bogumil, R. (1996) *NATO ASI Ser. 2/26*, 195−215.
17. Pederson, O. A., and Jacobsen, J. (1980) *Eur. J. Biochem. 105*, 291−295.
18. Hemmerich, P., and Sigwart, C. (1963) *Experientia 19*, 488−489.
19. Beltramini, M., and Lerch, K. (1983) *Biochemistry 22*, 2043−2048.
20. Winge, D. R. (1991) *Methods Enzymol. 205*, 458−469.
21. Stillman, M. J. (1992) in *Metallothioneins* (Stillman, M. J., Shaw, C. F., III, and Susuki, K. T., Eds.) pp 55−127, VCH Publisher, New York.
22. Li, Y.-J., and Weser, U. (1992) *Inorg. Chem. 31*, 5526−5533.
23. Pountney, D. L., Schauwecker, I., Zarn, J., and Vašák, M. (1994) *Biochemistry 33*, 9699−9705.
24. Ford, P. C., and Vogler, A. (1993) *Acc. Chem. Res. 26*, 220−226.
25. Byrd, J., Berger, R. M., McMillin, D. R., Wright, C. F., Hamer, D., and Winge, D. R. (1988) *J. Biol. Chem. 263*, 6688−6694.
26. Vašák, M., and Kägi, J. H. R. (1983) *Met. Ions Biol. Syst. 15*, 213−273.
27. Willner, H., Vašák, M., and Kägi, J. H. R. (1987) *Biochemistry 26*, 6287−6292.
28. Kull, F. J., Reed, M. F., Elgren, T. E., Ciardelli, T. L., and Wilcox, D. E. (1990) *J. Am. Chem. Soc 112*, 2291−2298.
29. Stillmann, M. J., Cai, W., and Zelazowski, A. J. (1987) *J. Biol. Chem. 262*, 4538−4548.
30. Maret, W., and Vallee, B. L. (1993) *Methods Enzymol. 226*, 52−71.
31. Vašák, M. (1980) *J. Am. Chem. Soc 102*, 3953−3955.
32. Carlin, R. L. (1965) in *Transition Metal Chemistry* (Carlin, R. L., Ed.) pp 1−33, Marcel Dekker, New York.
33. Holmquist, B., and Vallee, B. L. (1979) *Proc. Natl. Acad. Sci. U.S.A. 76*, 6216−6220.
34. Bertini, I., Luchinat, C., Messori, L., and Vašák, M. (1989) *J. Am. Chem. Soc. 111*, 7296−7300.
35. Good, M., Hollenstein, R., and Vašák M. (1991) *Eur. J. Biochem. 197*, 655−659.
36. Griffith, E. H., Hunt, G. W., and Amma, E. L. (1976) *J. Chem. Soc., Chem. Commun. 432*−433.
37. Nielson, K. B., Atkin, C. L., and Winge, D. R. (1985) *J. Biol. Chem. 260*, 5342−5350.
38. Oikava, S., Kurasaki, M., Kojima, Y., and Kawanishi, S. (1995) *Biochemistry 34*, 8763−8770.

BI9711994